Fiber-Optic Nanorefractometer Based on One-Dimensional Photonic-Bandgap Structures With Two Defects

Ignacio Del Villar, Ignacio R. Matías, *Senior Member, IEEE*, Francisco J. Arregui, *Member, IEEE*, and Richard O. Claus, *Senior Member, IEEE*

Abstract—A theoretical analysis of a fiber-optic photonic-bandgap (PBG)-based nanorefractometer is presented. Changes up to 11.2 dB in the optical output power in an index of refraction range of 1.7 with a sensitivity of $1.5 \cdot 10^{-4}$ have been demonstrated. The design is based on a one-dimensional PBG structure with two defects, which originates two defect states inside the bandgap. These states correspond to two localized modes in the defects. By selecting adequate parameters, the frequency of one of the localized modes can be fixed at the same time that its peak amplitude varies with the refractive index of the defect associated to the other localized mode. The refractive index of the defect associated to the localized mode that has been fixed in frequency remains constant. This enables a detection scheme based on a simple photodetector instead of an optical spectrum analyzer, as usual. The thickness of the defect whose refractive index varies determines the variation range of the transmitted power amplitude peak of the localized mode fixed at a concrete frequency. In addition, an analysis of the nonlinear dependence on the refractive index of the peak-transmitted power of the localized mode fixed at a concrete frequency is presented.

Index Terms—Coupled-mode analysis, electrostatic self-assembled (ESA), gratings, nanocavities, nanomaterials, optical-fiber transducers, photonic bandgap (PBG).

I. INTRODUCTION

THE importance of nanotechnology for future photonic devices and systems is well recognized. This multidisciplinary science domain represents an unprecedented challenge in research. Nanotechnology is bringing benefits to photonics, biotechnology, electronics, materials, information, and telecommunications, just to mention a few [1]–[4]. Photonic crystals of self-assembled colloids have generated great interest in the scientific community [5]–[10]. With suitable periodicities, symmetries, and dielectric contrasts, photonic crystals can exhibit stopbands or full bandgaps at optical or near-infrared wavelengths, making them attractive for applications such as optical switches, filters, and waveguides [10]–[16]. The introduction of a defect in a photonic-bandgap (PBG) structure has been analyzed thoroughly in the literature due to the possibility it presents that a defect state, corresponding to a localized mode in the defect, exist inside the range of forbidden wavelengths [16]–[19]. This property is frequently applied to one-dimensional (1-D) PBG structures because of its much easier fabrication. In this concrete case, the structure is considered by many authors in terms of Bragg gratings [13], [20]. However, in this paper, considerations will be taken from the point-of-view of PBG structures in order to facilitate the extrapolation of the theory explained in this study for applications where two- and three-dimensional structures are utilized. The position of the localized mode inside a bandgap is defined by the thickness and refractive index of the defect, being possible that it leaves the bandgap or that more than one localized mode be created if the thickness of the defect exceeds a limit value [12], [14], [16]. In this paper, the effect of two defects present in a 1-D PBG structure is analyzed. In this case, two localized modes are created inside the bandgap and the thickness and refractive index of the defects influence their position. It is also possible that both of them leave the bandgap or that more than one localized mode be created for each one if the thickness limit value is exceeded.

II. ELECTROSTATIC SELF-ASSEMBLED (ESA) MONOLAYER PROCESS

The ESA monolayer process is a technique used to build up coatings on a variety of different substrate materials such as ceramics, metals, and polymers of different shapes and forms, including planar substrates, prisms, and convex and concave lenses. In this paper, the applicability to a fiber-optic substrate for the aim of creating a fiber-optic device is shown in Section IV.

This method is based on the construction of molecular multilayers by the electrostatic attraction between oppositely charged polyelectrolytes in each monolayer deposited, and involves several steps [21]. The ESA film-deposition method is described schematically in Fig. 1.

First, a substrate (in this case, the optical fiber) is cleaned and treated to create a charged surface. The substrate is then exposed to a solution of a polyion of opposite charge for a short time (minutes) and, by adsorption, a monolayer of polyions is formed on the surface. In this way, the substrate is alternately
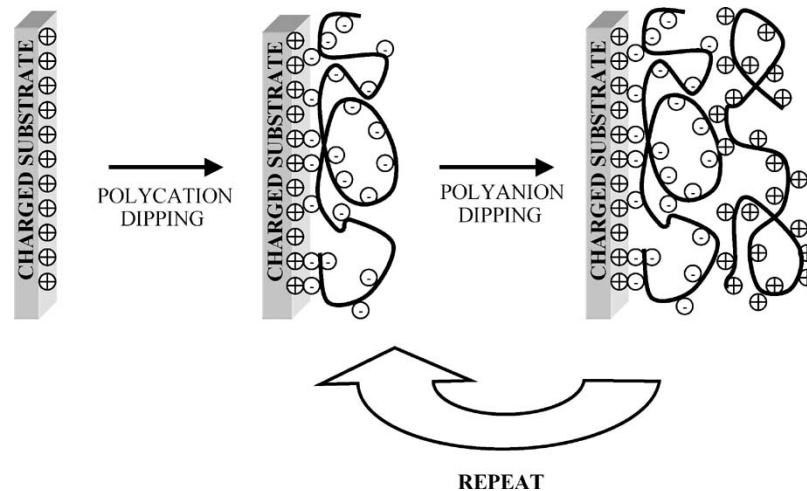
Fig. 1. Schematic of ESA deposition process.

dipped into solutions of cationic and anionic polymers (or appropriately charged inorganic clusters) to create a multilayer thin film, a polyanion–polycation multilayer. After each monolayer is formed, we rinse the sample in pure water to remove the excess of molecules that are not bound and that do not contribute to the monolayer structure.

The molecular species of the cationic and anionic components and the long-range physical order of the layers determine the resulting coating properties. It is important to notice that the polyanions and polycations overlap each other at the molecular level, and this produces a homogeneous optical material [21]. The individual layer composition and thickness can be controlled and substrates may include metals, plastics, ceramics, and semiconductors.

The versatility of the ESA method for the synthesis of materials permits the application of this technique to the design or fabrication of different optical fiber devices such as nanoFabry–Perot interferometers [9], fiber-optic gratings [10], or PBG structures [15]. The same type of structures could be used to develop optical-fiber sensors [22]. Fig. 2 shows three possible coatings to develop either fiber-optic sensors or devices in a reflective configuration. Devices using transmissive configurations can be implemented using the same structures, but changing air by silica (optical fiber) in Fig. 2. In Sections III and IV, the application of the ESA method in the construction of a 1-D PBG structure in a transmissive configuration will be detailed.

III. ANALYSIS OF 1-D PBG STRUCTURES WITH TWO DEFECTS

It is well known that, in a PBG structure, high-frequency propagating modes are attached to low refractive-index regions and that low-frequency propagating modes are attached to high refractive-index regions [16]. This conclusion is obtained from the electromagnetic variational theorem. The electromagnetic energy functional is minimized by the lowest electromagnetic mode. At the same time, to minimize the electromagnetic energy functional, the mode will tend to concentrate its displacement field in regions of high refractive index. This explains that low-frequency propagating modes are attached to high refractive-index regions, and the opposite can be justified in a similar
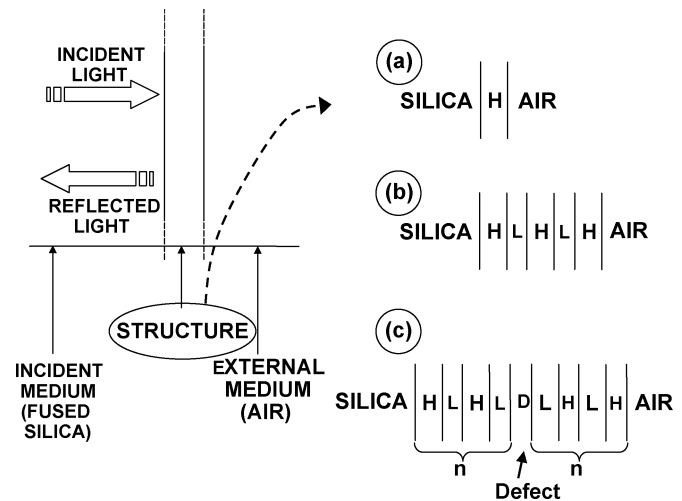

Fig. 2. Three possible coating structures to fabricate optical-fiber-based devices or sensors using the ESA method in a reflexive configuration scheme. (a) NanoFabry-Perot interferometers. (b) Optical-fiber gratings. (c) PBG structures on fiber.

way. Consequently, this theory can be extended to defect states that origin localized modes in the defects of the PBG structure. The change of properties of one defect will only affect the shift in frequency of one of the localized modes if they are sufficiently separated in the frequency spectrum by means of an important refractive index contrast between two defects. Nonetheless, the amplitude peak of the localized mode whose frequency remains constant (fixed localized mode) will be modified as the other one shifts its frequency inside the bandgap. The coupling of the two localized modes provokes this effect. If their frequencies are closer to each other, the coupling is better and the transmitted power of the fixed localized mode will be greater. This will yield to an intensity-based detection scheme, less expensive and more robust than a wavelength detection one, as normally used.

The example presented for the purpose of analyzing the presence of two defects in a 1-D PBG structure is that of Fig. 3. It is similar to that of [12] with the exception that there are 60 layers with the inclusion of two defects; one in the 20th layer and another one in the 40th layer. The optical thickness of each layer is λ quarter with λ 1550 nm. The reason for discarding
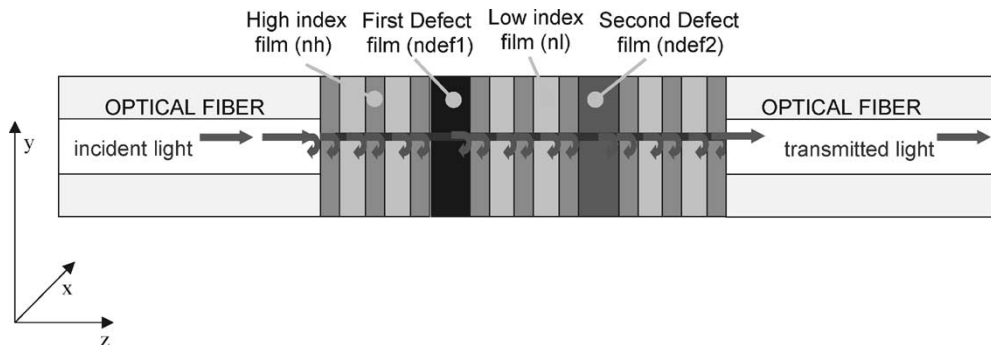
Fig. 3.   1-D-PBG structure of 60 layers with two defects.

the selection of a symmetrical structure of 59 layers is that the modes are more coupled and, only for a really great contrast of refractive indexes, can the fixing in frequency of one of the localized modes and a variation of the peak transmitted power of this fixed localized mode be achieved. The thickness of both of them is 100 nm, in order to avoid the creation of more than two localized modes, which begins at thickness values that exceed 200 nm [14]. A value close to the limit is selected because the thickness of a defect layer is also responsible for the wavelength shift of the localized mode. The higher the thickness value is, the greater shift in frequency the defect mode will present [12], [14]. With two examples in Section IV, it will be proven that the increase in thickness causes higher variations in the peak transmitted power of the fixed localized mode. This improves the sensitivity of the device against different refractive indexes.

In the first design presented, the refractive index of the first defect will present a value of one, whereas that of the second one will be varied from 1.8 to 3.5. Nevertheless, there are concrete designs where even though an additional localized mode is created, due to the increase in thickness of the defect layer, one of the two defects attached to the defect layer leaves the bandgap. In this case, considered in the second design of this study, it will be also assured that only two localized modes exist inside the bandgap, which is the aim of this study. In this last case, the refractive index of the first defect will be fixed to a value (3.376), whereas the value of the second one will vary from 1 to 2. Both refractive index values 1 and 3.376 are theoretical to show extreme cases where the fine properties of this design can be better understood. Today, refractive index values that range from 1.4 to 2.7 can be applied. This permits the detection of a wide range of refractive indexes. The simulation of the transmission in this structure is obtained with a program based on the rigorous coupled-wave analysis (RCWA) [23] (see the Appendix). The structure is considered as a stack of layers of different thicknesses and refractive indexes in the z axis. In both the x and y axes, the Fourier expansion of the permittivity is a constant because the material is homogeneous in both directions. As a first example, the design proposed here will be simulated for a total of 5000 points in the wavelength range between 1500–1750 nm, where the main bandgap centered at 1550 nm is located. There are other bandgaps located at lower wavelengths that are submultiples of 1550 nm. They can be considered as harmonics of the main bandgap. The second defect has a refractive index of one. In Fig. 4, it can be appreciated that, as the refractive index of the first defect increases, the wavelength shift of the local-
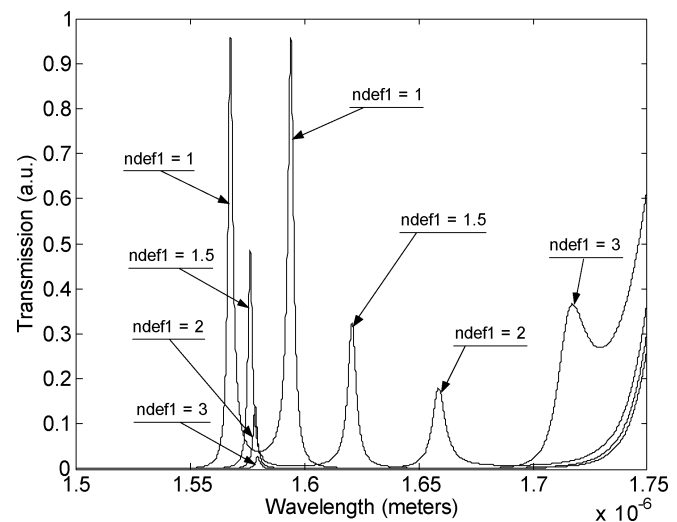

Fig. 4.   Transmitted power plot for four different refractive indexes in the first defect. The refractive index of the second defect is fixed to one (air).

ized mode located at 1567 nm decreases until it reaches a fixed value at 1580 nm. At this point, only its peak amplitude gets modified because there is an important contrast between the refractive index of both defects. Notice that both the value of the wavelength and the peak amplitude of the first localized mode also get modified as the refractive index of the first defect is varied.

This effect could also be obtained by adequate parameterization of the thickness because it also defines the frequency of the localized mode. Nevertheless, it owns the undesired property that, if a limit value is exceeded, more defects appear. This phenomenon is obeyed under a quantization of the modes. Light is bounced back and forth in a cavity with a thickness of the order of optical communication wavelength. Mirrors surround this cavity. As the thickness of the cavity is increased, more modes are quantized [16]. In addition to this, the dependence of high- or low-frequency modes with the thickness is not as clear as with the refractive index.

IV. APPLICATION IN A FIBER-OPTIC-BASED NANOREFRACTOMETER

Here, two different designs based on the same structure as that of Fig. 3 will be shown. One is for detecting refractive index changes from 1 to 2 with sensitivity and optical range of $5.6 \cdot 10^{-4}$ and 1.8 dB, respectively. The other one is for
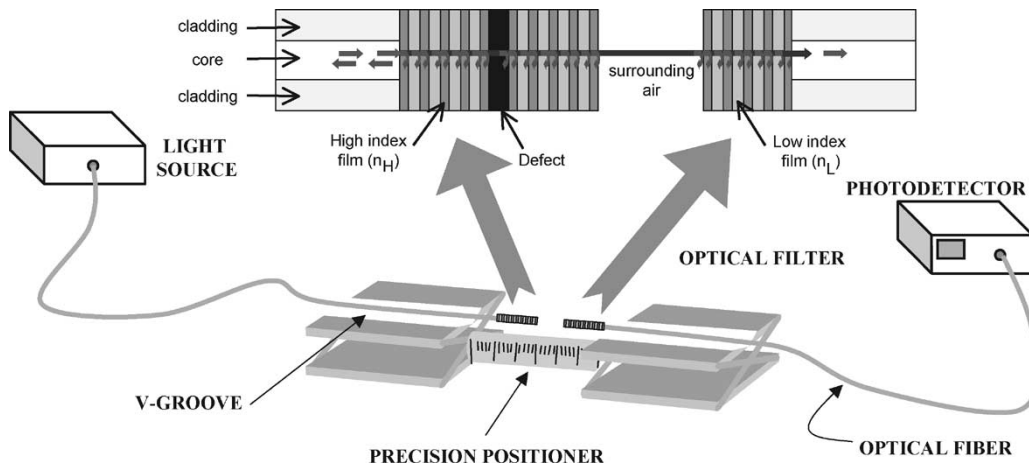
Fig. 5.   Configuration setup of the fiber-optic-based nanorefractometer. 1-D PBG structure of 60 layers with two defects.

higher refractive index values with sensitivity and optical range of $1.5 \cdot 10^{-4}$ and 11.2 dB, respectively. The sensitivity is defined based on a photodetector with a precision of 0.001 dBm. Considering the range of detected powers for different refractive indexes in the variable refractive index layer, the sensitivity of the device can be obtained. Changing several parameters in the design, it is possible to fabricate any other refractometer for any application. This opens up the use of the design rules explained here to develop *ad hoc* refractometers.

The structure of Fig. 5 will be used for the first optical-fiber PBG-based refractometer. In this case, the detection scheme will be a simple photodetector filtered at the wavelength of the localized mode. We want to analyze the transmitted power at this wavelength in order to detect changes in the refractive index.

With regard to the deposition of layers onto the extreme of optical-fiber pigtails, preliminary experiments have been successfully developed by using the ESA fabrication method [10]. Two fibers will be placed face-to-face by a precision positioner. At the end of one of them, there will be a stack of 39 layers, the middle one being a defect of a material with a refractive index similar to air. At the end of the other fiber pigtail, 19 layers will be stacked. The separation between both fiber pigtails will constitute the other defect that will be covered by the material to be measured. The two types of layers present apart from the defect layer have a refractive index of $n_H = 1.8$ (corresponding to $[\text{Au} : \text{PDDA}^+/\text{PSS}^-]^n$ bilayers) [9], and $n_L = 1.424$ (corresponding to $[\text{Poly R} - 478\,\text{PDDA}^+/\text{PSS}^-]^n$ bilayers) [8]. So as to avoid the ripple analyzed in [12], an index matching gel can be applied between both the fiber and light source and, on the other hand, between the photodetector and fiber.

With the design proposed and the parameters of the 1-D PBG structure analyzed in Section III, it can be observed in Fig. 6 that the wavelength of the first localized mode remains constant from high to low indexes for values higher than 1.8. In order to show that the effect explained in Section III can be applied independent of the order of the defects, in this case, the refractive index of the first defect will be one. The second one will be varied, which is the opposite of that shown in the design of Fig. 4. For refractive indexes 2.458 (ZnSe), 2.735 (ZnTe), and 3.376 (GaAs), the shift in frequency is unappreciable, whereas at 1.8 ($[\text{Au} : \text{PDDA}^+/\text{PSS}^-]^n$), a slight shift begins, which is
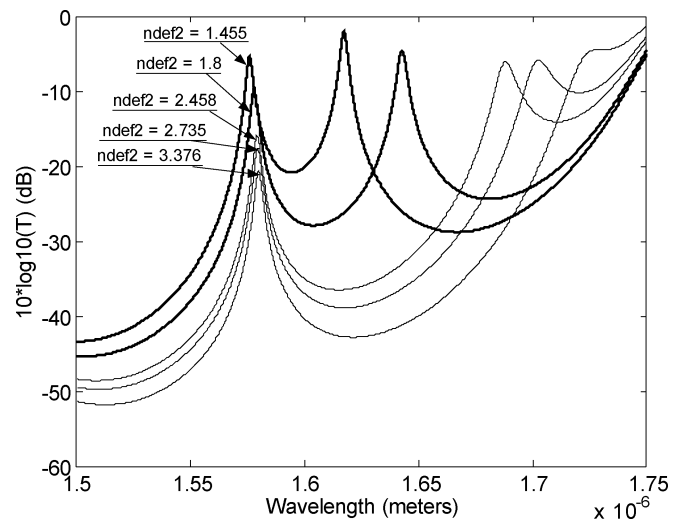

Fig. 6.   Transmitted power plot in logarithmic scale for four different refractive indexes in the second defect. The refractive index of the first defect is fixed to a value of one (air).

highly increased at a refractive index of coconut oil: 1.455 [24]. This effect is shown in Fig. 6.

It is important to analyze the linearity of the increase in the peak transmitted power of the fixed localized mode in order to know if a further signal conditioning will be required. This is analyzed in Fig. 7. The relative change in the peak transmitted power of the fixed localized mode related to the case of refractive index 1.8 is represented for the range of refractive indexes between 1.8 and 3.5. This is the range where this first refractometer is to work properly.

The increase of the peak-transmitted power of the localized mode is not linear, but this nonlinearity can nearly be suppressed with a common logarithmic treatment. Fig. 7 indicates that a photodetector could distinguish values of the refractive index of $1.5 \cdot 10^{-4}$. This may advantageously compete with commercial refractometers that present similar values between 10^{-4} and 10^{-5}, but with lower ranges of refractive indexes from 0.2 to 0.4 units. This is the point where the design proposed in this study is more advantageous.

In order to demonstrate the flexibility in the design of these types of structures, another design is proposed in this paper cov-
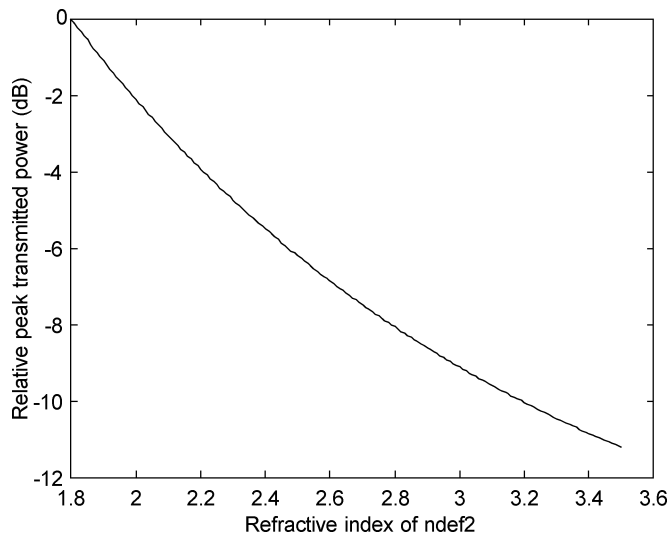
Fig. 7. Relative change in the peak-transmitted power of the fixed localized mode for the range of refractive indexes of the refractometer design of Fig. 6. The peak transmitted power taken as a reference is the one correspondent to a structure with a second defect of refractive index 1.8.
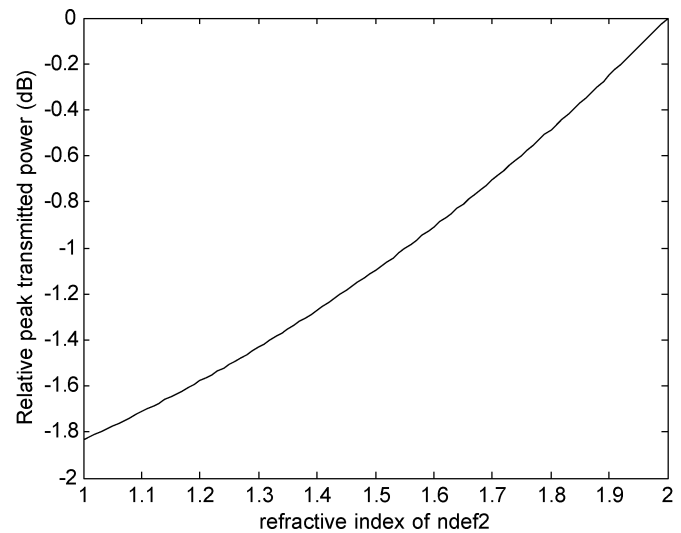

Fig. 9. Relative change in the peak-transmitted power of the fixed localized mode for the range of refractive indexes of the refractometer design of Fig. 8. The peak transmitted power taken as a reference is the one correspondent to a structure with a second defect of refractive index 2.
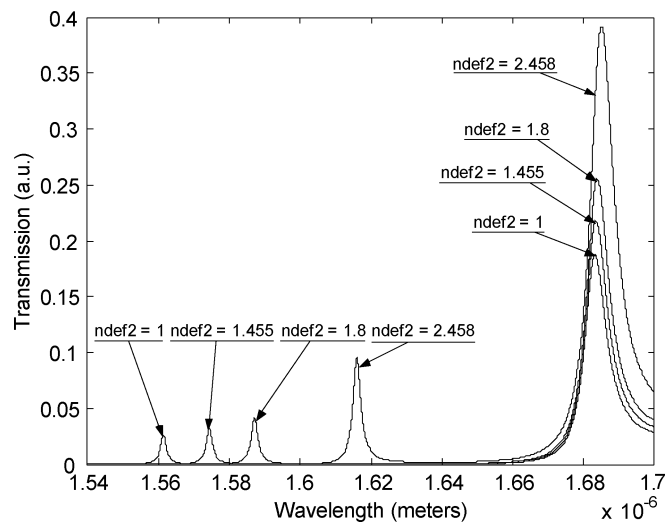

Fig. 8. Transmitted power plot for four different refractive indexes in the second defect. The first defect is fixed to 3.376 (GaAs).

ering a different range of indexes. The first defect will have a refractive index value of 3.376, which corresponds to GaAs. The second one will vary from 1 to 2, yielding to a change in the output optical power of the fixed localized mode.

The following our refractive indexes have been represented in Fig. 8:

1) air (1);
2) coconut oil (1.455);
3) $[Au : PDDA^+/PSS^-]$ (1.8);
4) ZnSe (2.458).

The design in this case requires that the thickness of the first defect be 300 nm, and the thickness of the second one be 40 nm. Due to the low thickness of the defect whose refractive index is getting varied, the shift in frequency of its localized mode will be not so important as in the other design. Consequently, the transmitted power of the fixed localized mode will not vary so much. In other words, the decoupling of the two localized modes

will be slower in terms of a change in the refractive index of the second defect, and the sensitivity of the device will be reduced.

Another design with a greater thickness of the second localized mode could be possible, but the shift in frequency would be so wide that not all refractive indexes from 1 to 2 could be analyzed. The localized mode whose frequency varies with the refractive index of the defect would leave the bandgap and another localized mode would be included. As this localized mode shifts from lower to higher wavelengths, it would couple the fixed localized mode. As a result, the wavelength of this mode would change, leading to a wrong detection in the photodetector of the variation in the peak-transmitted power.

In this design, the linearity of the increase of the peak transmitted power of the localized mode for different refractive indexes has been also analyzed in Fig. 9. Again, a logarithmic analysis leads to a nearly linear plot. As explained above, in this second example, the sensitivity is slightly slower than in the other one. Regardless, refractive index differences of $5.6 \cdot 10^{-4}$ can be distinguished.

It is also important to remark that, with this type of design, it is possible to decide not only the working range of indexes of refraction, but also the slope and the sign of the slope of the working curve (see Figs. 7 and 9). This is important for its use in real and quite different and wide applications.

V. CONCLUSION

It has been analyzed in this paper that the presence of two defects in a 1-D PBG structure can lead to the creation of two localized modes. By applying two refractive indexes quite different for the defects, it can be achieved that both defect modes are not attached to each other. The frequency of one of them can be fixed for a wide range of refractive indexes with a change in the amplitude peak of the localized mode. This can be used for the aim of designing a fiber-optic PBG-based nanorefractometer. Two designs have been presented that adequate for both high and low indexes, respectively. Further signal conditioning will be necessary

because it has been analyzed that the dependence between the refractive index of the defect and the peak-transmitted power of the fixed localized mode is not linear. The degree of flexibility in the design (because it is possible to select the measurement range), optical range, slope, sign of the slope of the working curve, etc. has also been shown. This constitutes an improvement of the other 1-D PBG or Bragg-grating-based devices because, in this case, there is no need of an optical spectrum analyzer.

APPENDIX

The RCWA is a modal method by Fourier expansion that permits to simulate PBG structures formed by stacks of homogeneous, grating, and bi-grating layers [23]. The structures analyzed in this study are formed by stacks of homogeneous layers of thickness much lower than the diameter of the fiber itself. This permits the approximation of the structure as homogeneous and infinite in both the x and y axes, shown in Fig. 3. Finally, the magnetic and electric fields can be explained by means of a modal expansion.

There are six steps in the development of the RCWA algorithm, which are as follows.

Step 1) Decomposition of the structure into homogeneous, grating, and bi-grating layers so as to perform a layer-by layer treatment. Here, the structure will be decomposed into the different types of homogeneous layers.

Step 2) Fourier expansion of the permittivity in the different types of layers. If the layer is homogenous in both the x and y axes, there is only a dc component, which is the case in the structure analyzed in this study.

Step 3) Plane-wave 1-D expansion of Maxwell equations, which gives, as a result, a set of two coupled-wave equations, expressed with a coupled matrix that relates the components of both magnetic and electric fields at both sides of each layer.

For the TE mode, the transfer matrix is

$$\begin{bmatrix} \dfrac{\partial S_y}{\partial z} \\ \dfrac{\partial U_x}{\partial z} \end{bmatrix} = k_0 \begin{bmatrix} 0 & I \\ K_X^2 - E & 0 \end{bmatrix} \cdot \begin{bmatrix} S_y \\ U_x \end{bmatrix} \quad (1)$$

and, for the TM mode, the transfer matrix is

$$\begin{bmatrix} \dfrac{\partial U_y}{\partial z} \\ \dfrac{\partial S_x}{\partial z} \end{bmatrix} = k_0 \begin{bmatrix} 0 & E \\ K_X E^{-1} K_X - I & 0 \end{bmatrix} \cdot \begin{bmatrix} U_y \\ S_x \end{bmatrix} \quad (2)$$

where I is the identity matrix, K_X is a diagonal matrix whose diagonal elements are the normalized wave vectors in the x axes of the corresponding diffraction orders extracted from the Floquet theorem, E is the matrix formed by the permittivity harmonic coefficients of the expansion in Step 2), and S and U are vectors formed by the space–harmonic coefficients proportional to those of the magnetic and electric fields.

Step 4) Determination of the eigenvalues and eigenvectors of the coupling matrix for the different types of layers.

Step 5) Deduction of the formula that calculates the components of vectors of the transmitted and reflected fields by matching conditions outside the structure.

Step 6) Calculation of the diffraction efficiencies and the total transmitted and reflected power for the range of wavelengths analyzed.

The problem of convergence disappears for 1-D PBG structures and it must be remarked that both the TE and TM modes will coincide, consequently, only the analysis of one of them is necessary. This implies an important improvement in the efficiency of the algorithm. Other computational time reductions can be found in [23]. Regarding the instability problems, they are avoided by using the S- or R-matrix algorithm. Both of them are compared in [25].

After the resolution of these problems, it can be asserted that the RCWA method is adequate for the simulation of the 1-D PBG structures proposed in this study because it achieves accurate results in comparison to the rest of methods, only overcome by modal methods by modal expansion, which can only simulate those profiles that are continuous [26]. In the structures considered here, the accuracy achieved by the RCWA method is the same as the modal method by modal expansion (MMME) methods because the Fourier expansion of the permittivity for each layer produces no error. This is due to fact that, in this case, all layers are homogeneous. As a result, there is only a dc component, which also makes this method algebraically equivalent to a Fresnel approach. In addition to this, the method is really versatile and permits to introduce any defect with different properties in any position by changing some parameters in the algorithm. The applicability of this method toward analysis of waveguides has been proven by numerous authors [27], [28].

REFERENCES

[1] M. T. Bohr, "Nanotechnology goals and challenges for electronic applications," *IEEE Trans. Nanotechnol.*, vol. 1, pp. 56–62, Mar. 2002.

[2] T. A. Desai, D. J. Hansford, L. Kulinsky, A. H. Nashat, G. Rasi, J. Tu, Y. Wang, M. Zhang, and M. Ferrari, "Nanopore technology for biomedical applications," *Biomed. Microdevices*, vol. 2, pp. 11–40, 1999.

[3] A. Scherer, O. Painter, J. Vuckovic, M. Loncar, and T. Yoshie, "Photonic crystals for confining, guiding, and emitting light," *IEEE Trans Nanotechnol.*, vol. 2, pp. 4–11, Mar. 2002.

[4] S. Muthukumar, H. Sheng, J. Zhong, Z. Zhang, N. W. Emanetoglu, and Y. Lu, "Selective MOCVD growth of ZnO nanotips," *IEEE Trans. Nanotechnol.*, vol. 2, pp. 50–54, Mar. 2002.

[5] Y. Liu, Y. Wang, and R. O. Claus, "Layer-by-layer ionic self-assembly of Au colloids into multilayer thin-films with bulk metal conductivity," *Chem. Phys. Lett.*, vol. 298, pp. 315–319, 1998.

[6] K. D. Harris, J. C. Sit, and M. J. Brett, "Fabrication and optical characterization of template-constructed thin films with chiral nanostructure," *IEEE Trans. Nanotechnol.*, vol. 1, pp. 122–128, Sept. 2002.

[7] E. Delamarche, B. Michel, C. Gerber, D. Anselmetti, H.-J. Guentherodt, H. Wolf, and H. Ringsdorf, "Real-space observation of nanoscale molecular domains in self-assembled monolayers," *Langmuir*, vol. 10, pp. 2869–2871, 1994.

[8] F. J. Arregui, B. Dickerson, R. O. Claus, I. R. Matías, and K. L. Cooper, "Polymeric thin films of controlled complex refractive index formed by the electrostatic self-assembled monolayer process," *IEEE Photon. Technol. Lett.*, vol. 13, pp. 1319–1321, Dec. 2001.

[9] F. J. Arregui, Y. Liu, K. M. Lenahan, I. R. Matías, and R. O. Claus, "Optical fiber nanometer-scale Fabry Perot interferometer formed by the ionic self-assembly monolayer process," *Opt. Lett.*, vol. 24, pp. 596–598, 1999.

[10] F. J. Arregui, I. R. Matías, K. L. Cooper, and R. O. Claus, "Fabrication of microgratings on the ends of standard optical fibers by electrostatic self-assembly monolayer process," *Opt. Lett.*, vol. 26, pp. 131–133, 2001.

[11] P. Mach, P. Wiltzius, M. Megens, D. A. Weitz, K.-H. Lin, T. C. Lubensky, and A. G. Yodh, "Electro-optic response and switchable Bragg diffraction for liquid crystals in colloid-templated materials," *Phys. Rev. E, Stat. Phys. Plasmas Fluids Relat. Interdiscip. Top.*, vol. 65, pp. 720–723, 2002.

[12] I. Del Villar, I. R. Matías, F. J. Arregui, and R. O. Claus, "Analysis of 1D-PBG structures with a liquid crystal defect toward development of fiber-optic tunable wavelength filters," *Opt. Exp.*, vol. 11, pp. 430–436, 2003.

[13] A. Meloni, M. Chinello, and M. Martinelli, "All optical switching in phase-shifted fiber Bragg grating," *F. Tech. Lett.*, vol. 12, pp. 42–44, 2000.

[14] I. R. Matías, I. Del Villar, F. J. Arregui, and R. O. Claus, "Development of an optical refractometer by analysis of one-dimensional photonic bandgap structures with defects," *Opt. Lett.*, vol. 28, pp. 1099–1101, 2003.

[15] P. Tran, "Optical switching with a nonlinear photonic crystal: A numerical study," *Opt. Lett.*, vol. 21, pp. 1138–1140, 1996.

[16] J. D. Joannopoulos, R. D. Meade, and J. N. Winn, *Photonic Crystals: Molding the Flow of Light*. Princeton, NJ: Princeton Univ. Press, 1995.

[17] E. Yablonovitch, "Photonic bandgap structures," *J. Opt. Soc. Amer. B, Opt. Image Sci.*, vol. 10, pp. 283–295, 1993.

[18] P. Dansas and N. Paraire, "Fast modeling of photonic bandgap structures by use of a diffraction-grating approach," *J. Opt. Soc. Amer. A, Opt. Image Sci.*, vol. 15, pp. 1586–1598, 1998.

[19] O. Painter, R. K. Lee, A. Yariv, A. Scherer, J. D. O'Brien, P. D. Dapkus, and I. Kim, "Two-dimensional photonic crystal defect laser," *Science*, vol. 284, pp. 1819–1821, 1999.

[20] T. Erdogan, "Fiber grating spectra," *J. Lightwave Technol.*, vol. 15, pp. 1277–1294, Aug. 1997.

[21] G. Decher, "Fuzzy nanoassemblies: Toward layered polymeric multicomposites," *Science*, vol. 277, pp. 1232–1237, 1997.

[22] I. R. Matías, I. Del Villar, F. J. Arregui, and R. O. Claus, "Molecularly self-assembled optical fiber sensors," in *Proc. 1st IEEE Sensors Conf.*, 2002, pp. 198–202.

[23] ——, "Comparative study of the modeling of 3D photonic bandgap structures," *J. Opt. Soc. Amer. A, Opt. Image Sci.*, vol. 20, pp. 644–654, 2003.

[24] S. A. Khodier, *Opt. Laser Technol.*, vol. 34, p. 125, 2002.

[25] L. Li, "Formulation and comparison of two recursive matrix algorithms for modeling layered diffraction gratings," *J. Opt. Soc. Amer. A, Opt. Image Sci.*, vol. 13, pp. 1024–1035, 1996.

[26] L. Li and C. W. Haggans, "Convergence of the coupled-wave method for metallic lamellar diffraction gratings," *J. Opt. Soc. Amer. A, Opt. Image Sci.*, vol. 10, pp. 1184–1189, 1993.

[27] J. Tervo, M. Kuittinen, P. Vahimaa, J. Turunen, T. Aalto, P. Heimala, and M. Leppilhalme, "Efficient Bragg waveguide grating analysis by quasirigorous approach based on Redheffers's star product," *Opt. Commun.*, vol. 198, pp. 265–272, 2001.

[28] E. Silberstein, P. Lalanne, J. P. Hugonin, and Q. Cao, "Use of grating theories in integrated optics," *J. Opt. Soc. Amer. A, Opt. Image Sci.*, vol. 18, pp. 2865–2875, 2001.

Ignacio R. Matías (M'01–SM'03) received the M.S. degree in electrical and electronic engineering and Ph.D. degree (with a specialty in optical fiber sensors) from the Polytechnic University of Madrid (UPM), Madrid, Spain, in 1992 and 1996, respectively.

In 1996, he joined the Public University of Navarra, Pamplona, Spain, where he is currently a Professor. He has coauthored over 100 journal and conference papers related to optical fiber sensors, passive optical devices, and systems.
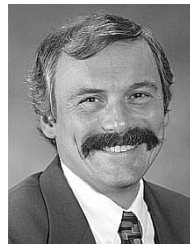
Dr. Matías is an associate editor for the IEEE SENSORS JOURNAL.

Francisco J. Arregui (M'01) received the M.S. degree in electrical engineering from the Catholic University of Navarra, San Sebastian, Spain, in 1994, and the Ph.D. degree from the Public University of Navarra, Pamplona, Spain, in 2000.

He has been a member of the Centro de Estudios e Investigaciones Técnicas (CEIT) Research Center, San Sebastian, Spain, for two years and has been involved in numerous projects with industry including medical instrumentation, monitoring of high-power lines, and communications hardware. Since 1995, he has been with the Public University of Navarra, Pamplona, Spain. During 1998 and 2000, he was a Visiting Scientist with the Fiber and Electro Optics Research Center, Virginia Polytechnic Institute and State University, Blacksburg, VA. His main research interests include optical-fiber sensors, sensor materials, and nanostructured materials. He has served as a referee for *Optical Engineering*, *Sensors and Actuators A*, and *Optics Communications*.

Dr. IEEE Arregui is a member of The International Society for Optical Engineers (SPIE). He has served as reviewer for the IEEE PHOTONICS TECHNOLOGY LETTERS and the IEEE SENSORS JOURNAL.

Ignacio Del Villar received the M.S. degree in electrical and electronic engineering from the Public University of Navarra (UPNA), Pamplona, Spain, in 2002, and is currently working toward the Ph.D. degree in electrical and electronic engineering from the UPNA.

His research interest include optical-fiber sensors and the analysis of PBG structures.

Richard O. Claus (S'73–M'77–SM'83) received the B.E.S. and Ph.D. degrees in electrical engineering from The Johns Hopkins University, Baltimore, MD, in 1973 and 1977, respectively.

Since 1977, he has been a member of the faculty with the Virginia Polytechnic Institute and State University, Blacksburg, where he is currently the Hester Chair of Engineering and the Director of the Fiber and Electro-Optics Research Center. His current interests are optical-fiber sensors and self-assembled materials and structures.

Dr. Claus is a Fellow of the Institute of Physics (IOP) and The International Society for Optical Engineers (SPIE). He has been the recipient of numerous awards for the application of optical-fiber sensors for materials analysis from the American Society of Civil Engineers (ASCE), the American Society of Mechanical Engineers (ASME), the Optical Society of America (OSA), and the Instrument Society of America (ISA).